

Low-pH-Induced Lamellar to Bicontinuous
Primitive Cubic Phase Transition in
Dioleoylphosphatidylserine/Monoolein
Membranes

| | |
|-------|--|
| メタデータ | 言語: en 出版者: American Chemical Society 公開日: 2018-11-12 キーワード (Ja): キーワード (En): 作成者: Oka, Toshihiko, Hasan, Moynul, Islam, Md. Zahidul, Moniruzzaman, Md., Yamazaki, Masahito メールアドレス: 所属: |
| URL | http://hdl.handle.net/10297/00025889 |

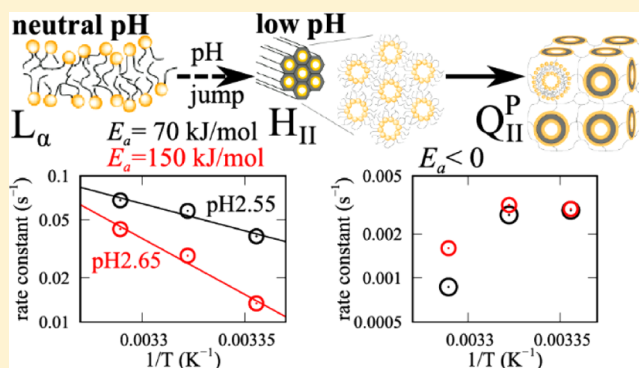
Low-pH-Induced Lamellar to Bicontinuous Primitive Cubic Phase Transition in Dioleoylphosphatidylserine/Monoolein Membranes

Toshihiko Oka,^{†,‡,Ⓢ} Moynul Hasan,[§] Md. Zahidul Islam,^{§,||} Md. Moniruzzaman,[§] and Masahito Yamazaki^{*,†,‡,§,Ⓢ}

[†]Nanomaterials Research Division, Research Institute of Electronics, [‡]Department of Physics, Graduate School of Science, and [§]Integrated Bioscience Section, Graduate School of Science and Technology, Shizuoka University, Shizuoka 422-8529, Japan

S Supporting Information

ABSTRACT: Electrostatic interactions (EIs) play important roles in the structure and stability of inverse bicontinuous cubic (Q_{II}) phases of lipid membranes. We examined the effect of pH on the phase of dioleoylphosphatidylserine (DOPS)/monoolein (MO) membranes at low ionic strengths using small-angle X-ray scattering (SAXS). We found that the phase transitions from lamellar liquid-crystalline (L_{α}) to primitive cubic (Q_{II}^P) phases in DOPS/MO (2/8 molar ratio) membranes occurred in buffers containing 50 mM NaCl at and below the final pH of 2.75 as the pH of the membrane suspension was decreased from a neutral value. The kinetic pathway of this transition was revealed using time-resolved SAXS with a stopped-flow apparatus. The first step is a rapid transition from the L_{α} phase to the hexagonal II (H_{II}) phase, and the second step is a slow transition from the H_{II} phase to the Q_{II}^P phase. We determined the rate constants of the first step, k_1 , and of the second step, k_2 , by analyzing the time course of SAXS intensities quantitatively. The k_1 value increased with temperature. The analysis of this result provided the values of its apparent activation energy, which were constant over temperature but increased with pH. This can be explained by an EI effect on the free energy of the transition state. In contrast, the k_2 value decreased with temperature, indicating that the true activation energy increased with temperature. These experimental results were analyzed using the theory of the activation energy of phase transitions of lipid membranes when the free energy of the transition state depends on temperature. On the basis of these results, we discussed the mechanism of this phase transition.



1. INTRODUCTION

Electrostatic interaction is one of the most important physical interactions in biological molecular systems, especially biomembranes such as plasma membranes and lipid membranes.^{1–5} Typically, biomembranes and lipid membranes are planar, lamellar membranes, which are in the liquid-crystalline (L_{α}) phase, but under certain conditions, they form regular three-dimensional (3D) structure membranes in inverse bicontinuous cubic (Q_{II}) phases, in which water channels with nanometer diameters were connected to each other.^{6–10} Recently, it has been well established that electrostatic interactions (EIs) due to surface charges of lipid membranes play various important roles in the structures and phase stabilities of the Q_{II} phases of biological lipid membranes. One of the EI effects on the Q_{II} phases is that the lattice constants and the size of water channels of the Q_{II} phase increase with an increase in the level of EI.^{11–15} The other EI effect is that the modulation of EI due to surface charges of membranes induces transitions between the L_{α} and Q_{II} phases and transitions between different Q_{II} phases in various lipids.^{11,12,16–34} As the surface charges, not only charged groups of hydrophilic segments of lipids but also charged side chains of amino

acids of peptides^{18,34} are used. Interactions of ions (such as H^+ and Ca^{2+}) and positively charged peptides also induced these phase transitions by changing the surface charge density of the membranes due to their binding to the charged groups.^{11,19,20,22,26,32}

Generally, to understand the characteristics of various phase transitions of lipid membranes and their mechanisms, information about their kinetic pathways is indispensable.^{35–41}

The first experimental evidence of the kinetic pathway of the EI-induced transition between the L_{α} and Q_{II} phase in lipid membranes has been revealed recently using time-resolved small-angle X-ray scattering (TR-SAXS); for the L_{α} to double-diamond Q_{II}^D (or Q^{224}) phase transition in a dioleoylphosphatidylserine (DOPS)/monoolein (MO) membrane induced by a decrease in pH, the first step is the direct transition from the L_{α} phase to a transient intermediate, an inverse hexagonal II (H_{II}) phase, and the second step is the slow transition from the H_{II} to Q_{II}^D phase.^{42,43} The rate constants of the two steps were

Received: July 19, 2017

Revised: September 28, 2017

Published: October 2, 2017

determined by the analysis of the time course of SAXS peak intensities.⁴³ The temperature dependence of the rate constants of this transition was also reported,⁴⁴ the rate constants of the first step and those of the second step at pH 2.7 and 2.8 increased with temperature, their analysis provided the apparent activation energies, but the rate constant at the second step at pH 2.6 decreased with temperature, suggesting its activation energy varies with temperature. These results were analyzed using the quantitative theory of the activation energy of phase transitions of lipid membranes, which was obtained by modification of the theory of Squires et al.,⁴⁵ including the effect of monolayer curvature. This new theory indicates that the free energy of the transition state depends on temperature and hence explains the results reasonably.⁴⁴

Generally, the activation energy of structural changes can provide valuable information about their elementary processes and mechanisms. One of the determinants of the activation energy is the free energy of the transition state. The temperature can change the free energy of the transition state of the phase transitions involved in the Q_{II} phases in lipid membranes.^{44,45} Currently, we have a hypothesis that the EI may control the free energy of the transition state.⁴⁴ In this report, to elucidate the EI effects on elementary processes of the L_{α} to Q_{II} phase transition in a DOPS/MO (2/8 molar ratio) membrane induced by a decrease in pH, we investigated this phase transition in the buffer containing 50 mM NaCl and also the temperature dependence of this phase transition. Debye lengths, measures of the effective length of electrostatic interaction, in a solution containing 50 and 100 mM NaCl are 1.4 and 0.96 nm, respectively.³ Therefore, we can reasonably expect that the EI in 50 mM NaCl is stronger than that in 100 mM NaCl, which was used in our previous investigation of the L_{α} to Q_{II} phase transition in a DOPS/MO (2/8) membrane induced by a decrease in pH.^{42–44} On the other hand, we demonstrated that the EI-induced transition between the L_{α} and Q_{II} phase in lipid membranes occurs mainly due to the change in the spontaneous curvature of monolayer lipid membranes.^{12,20,21,42,44} It is generally recognized that short-range forces such as interactions between headgroups of neighboring lipids strongly affect the spontaneous curvature of monolayers, which was verified by experimental results.^{18,19,46,47} Therefore, we can reasonably consider that the electrostatic interactions in the presence of 100 and 50 mM NaCl have strong effects on the spontaneous curvature of the monolayer. Furthermore, we consider that this stronger EI in 50 mM NaCl may more strongly affect the transition states of this phase transition. In this work, we first found that in the presence of 50 mM NaCl a transition from the L_{α} phase to the primitive Q_{II}^P (or Q^{229}) phase, not the Q_{II}^D phase, occurred as the pH of the membrane suspension was decreased from a neutral value. Next we investigated the kinetics of this transition using TR-SAXS with a stopped-flow apparatus and found that the L_{α} phase was directly transformed into the H_{II} phase during the first step and subsequently the H_{II} phase slowly converted into the Q_{II}^P phase. By analyzing these results, we determined the rate constants of the two elementary steps. Finally, we investigated the temperature dependence of this phase transition and obtained information about the activation energy of the two elementary steps.

2. MATERIALS AND METHODS

DOPS was purchased from Avanti Polar Lipids (Alabaster, AL). MO was purchased from Sigma-Aldrich Chemical Co. (St. Louis, MO). To

prepare DOPS/MO multilamellar vesicles (MLVs), we added 100 μ L of 10 mM ammonium acetate buffer (pH 6.7) containing 50 mM NaCl (buffer A) to a dry MO/DOPS lipid film (10 μ mol)⁴³ and then mixed the suspension several times using a vortex mixer for \sim 20 s at room temperature (\sim 25 $^{\circ}$ C). To purify MLVs, we centrifuged the MLV suspension at 13000g for 20 min at 25 $^{\circ}$ C and then resuspended the pellet gently in new buffer A without using the vortex mixer. This suspension was used as the purified MLV suspension. We used the purified MLVs within 12 h of preparation. We determined the lipid concentrations of the suspensions using the Bartlett method.⁴⁸ To measure the pH of DOPS/MO suspensions, a pH meter (HM-41X, DKK-TOA Co., Tokyo, Japan) was used, and the standard deviations of all the measured pH values were $<$ 0.03.

Data of temperature scanning SAXS were obtained at beamline BL-6A of the Photon Factory at KEK (Tsukuba, Japan), and the experimental methods have been described previously.⁴⁴ Immediately after the purified DOPS/MO MLV suspension in buffer A was mixed with 20 mM citrate buffer at various pH values containing 50 mM NaCl (buffer C) at a volume ratio of 1/9 in an Eppendorf tube, the resulting suspension was transferred into a quartz capillary tube with a diameter of 1.0 mm and a thickness of 0.01 mm (Hilgenberg GmbH, Malsfeld, Germany) and the ends of the tubes were sealed with silicone grease. This sample in the capillary was incubated for $>$ 5 h at \sim 25 $^{\circ}$ C before the SAXS measurement. After incubation of the sample in the capillary in the holder at 25 $^{\circ}$ C for 10 min, the temperature of the sample was increased from 25 to 50 $^{\circ}$ C at a rate of 1 K/min. During the temperature scan, the SAXS patterns were measured with a time resolution of 5 s. Lattice constants were determined by fitting two Gauss functions to (110) and (200) peaks of the Q_{II}^P phase and one to the (10) peak of the H_{II} phase. Peaks at larger angles were excluded from the fitting because their peak intensities were low. The positions of the peaks at larger angles were used in the phase determination of the samples.

We used the same method of TR-SAXS in our previous paper⁴⁴ to monitor structural changes in DOPS/MO membranes after the pH jump. TR-SAXS data were obtained at the BL40B2 beamline at SPring-8 (Sayo, Japan). A stopped-flow apparatus (SFM-CD10, UNISOKU, Osaka, Japan) was used to mix rapidly the purified DOPS/MO MLV suspension in buffer A with 20 mM citrate buffer at various pH values containing 50 mM NaCl (buffer C) at a volume ratio of 1/9. Other experimental conditions were described previously.⁴⁴

The lattice constant, a , of the Q_{II}^P phase is determined by the equation $S = (1/a)(h^2 + k^2 + l^2)^{1/2}$, and that of the H_{II} phase, which equals the center–center distance of adjacent cylinders in the H_{II} phase, is determined by the equation $S = [2/(3^{1/2}a)](h^2 + k^2 + hk)^{1/2}$, where S is the reciprocal spacing and h , k , and l are Miller indices. We used the non-negative matrix factorization (NMF) method based on a modified alternating least-squares (MALS) algorithm^{49,50} to obtain the time course of each phase in the SAXS patterns. The detailed method of analysis using the NMF method was described previously.⁴⁴

3. RESULTS

3.1. Effect of pH on the Structure of DOPS/MO Membranes in 50 mM NaCl. First, we examined the effect of pH on the structure of preformed DOPS/MO MLVs (2/8) in excess buffer containing 50 mM NaCl at 25 $^{\circ}$ C. The SAXS pattern of 5.0 mM purified MLVs of this membrane in ammonium acetate buffer (pH 6.7) showed a set of peaks with a spacing of 12 nm in a ratio of 1:2 (Figure 1a), indicating that it was in the L_{α} phase. We mixed various pH citrate buffers with the purified MLV suspension, and then the suspensions were incubated for 8–9 h before SAXS measurement. The final pH values of the suspensions were measured and are indicated in the texts and Figure 1. The structures of these samples greatly depended on the final pH of the suspension. For example, at a final pH of 2.55, the SAXS peaks that have a $\sqrt{2}:\sqrt{4}:\sqrt{6}:\sqrt{10}:\sqrt{12}:\sqrt{14}:\sqrt{16}:\sqrt{18}$ spacing ratio were

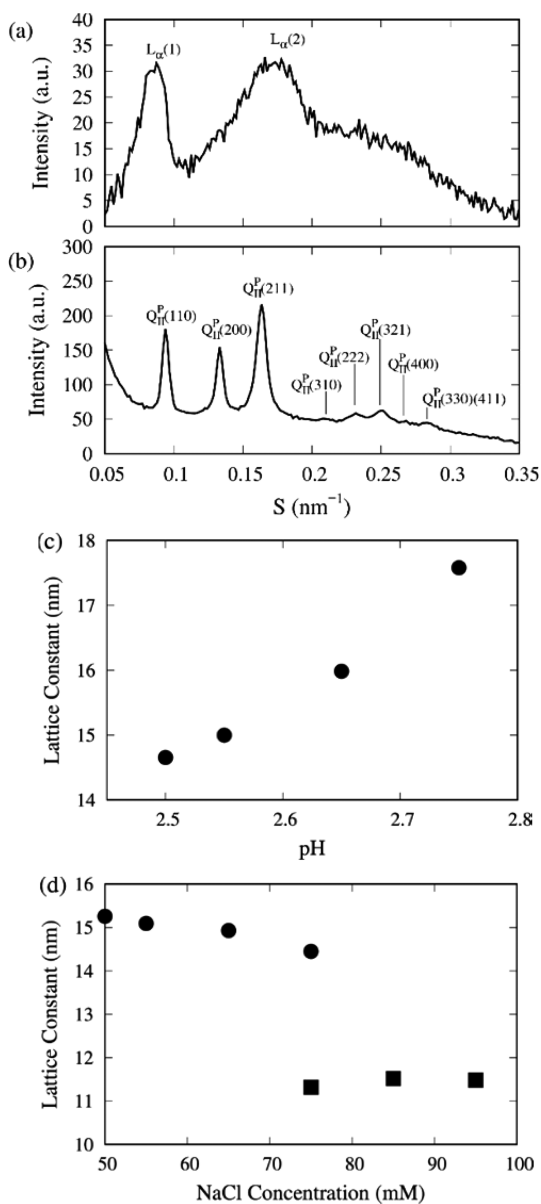


Figure 1. Dependence of the structure and phase of a DOPS/MO (2/8) membrane on pH and salt concentration. SAXS patterns of a DOPS/MO (2/8) membrane suspension (a) in buffer A (pH 6.7) containing 50 mM NaCl and (b) in mixed buffer at pH 2.55 containing 50 mM NaCl after a long incubation time of 10 h. (c) pH dependence of the lattice constant of the Q_{II}^P phase in a DOPS/MO (2/8) membrane in low-pH buffer containing 50 mM NaCl. (d) Dependence of the lattice constant and phase in a DOPS/MO (2/8) membrane on NaCl concentration at pH 2.6: (●) Q_{II}^P phase and (■) Q_{II}^D phase.

indexed as (110), (200), (211), (310), (222), (321), (400), and (330) (411) peaks of the Q_{II}^P phase, a bicontinuous, body-centered cubic phase;¹² its lattice constant was 15.2 nm (Figure 1b). Figure 1c shows the pH dependence of the structure of DOPS/MO (2/8) membranes. At and below pH 2.75, they were in the Q_{II}^P phase, and its lattice constant increased with pH.

We also examined the effect of NaCl concentration on the phase and structure of DOPS/MO (2/8) membranes at a final pH of 2.6. The membranes were in the Q_{II}^P phase in the presence of low NaCl concentrations but in the Q_{II}^D phase at

higher NaCl concentrations, and a transition between the Q_{II}^P and the Q_{II}^D phases occurred at 75 mM NaCl (Figure 1d).

3.2. Kinetics of the L_{α} to Q_{II}^P Phase Transition Induced by Decreasing the pH.

First, we examined the kinetic pathway of the L_{α} to Q_{II}^P phase transition in DOPS/MO (2/8) membranes in the presence of 50 mM NaCl at 25 °C, which was induced by decreasing the pH of the suspension from neutral pH to pH 2.55 (final pH). After mixing a purified MLV suspension in buffer A with buffer C (pH 2.40) using the stopped-flow apparatus, we continuously monitored the structure of the membranes in the suspension (final lipid concentration of 5.3 mM, final pH of 2.55). Figure 2a shows the time course of its SAXS patterns. The SAXS patterns from 0.2 to 10 s corresponded to the L_{α} phase due to MLV structure

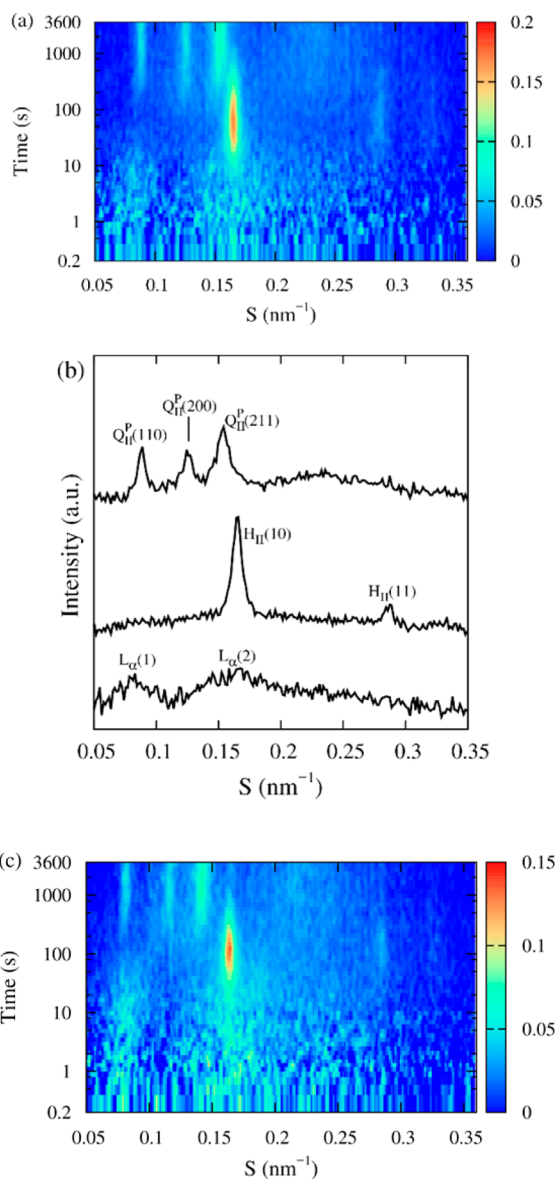


Figure 2. Changes in the structure and phase of DOPS/MO (2/8) membranes in 50 mM NaCl after the change in pH from pH 6.7 to a low pH at 25 °C. (a) SAXS contour plot of the time course at a final pH of 2.55. (b) Averaged SAXS patterns of the data shown in panel a from 0.2 to 9.2 s (bottom), from 50 to 89 s (middle), and from 2560 to 3629 s (top). (c) SAXS contour plot of the time course at a final pH of 2.65.

(Figure 2a,b). A new weak peak around $S = 0.167 \text{ nm}^{-1}$ was detected at $\sim 10 \text{ s}$, and its intensity grew over time. At 70 s , SAXS peaks with a spacing with a $1:\sqrt{3}:2$ ratio appeared (Figure 2a,b), corresponding to the H_{II} phase. Hence, we consider that the peak at $S = 0.167 \text{ nm}^{-1}$ was the (10) peak of the H_{II} phase. The peak intensities of the H_{II} phase grew over time to $\sim 70 \text{ s}$ and then decreased, while those of the L_{α} phase became low at $\sim 70 \text{ s}$. At $\sim 200 \text{ s}$, three weak peaks at 0.089 , 0.125 , and 0.154 nm^{-1} appeared, and their intensities grew over time (Figure 2a,b). The SAXS pattern of the same sample after 10 h was the same as that of Figure 1b, which corresponds to the Q_{II}^P phase as the equilibrium structure. Hence, we assigned the peaks at 0.089 , 0.125 , and 0.154 nm^{-1} in panels a and b of Figure 2 as the (110), (200), and (211) peaks of the Q_{II}^P phase, respectively. The analysis given above indicates that after the change in pH from a neutral value to a low value, the L_{α} phase converted into the H_{II} phase rapidly and then the H_{II} phase converted slowly into the Q_{II}^P phase.

We also examined the pH dependence of the kinetics of this transition. The qualitative kinetic pathways of the transitions at all pH values were the same as that at pH 2.55. Figure 2c shows that at a final pH of 2.65 a peak due to the H_{II} phase appeared $\sim 20 \text{ s}$ after mixing, and then the peaks due to the Q_{II}^P phase appeared $\sim 200 \text{ s}$ after mixing. The lattice parameters of the H_{II} and Q_{II}^D phases at pH 2.65 were larger than those at pH 2.55 (Table 1).

Table 1. Temperature Dependence of the Lattice Constants at Various pH Values

| temperature (°C) | L_{α} (initial) (nm) | H_{II} (intermediate) (nm) | Q_{II}^P (1 h) (nm) |
|------------------|-----------------------------|------------------------------|-----------------------|
| Final pH of 2.55 | | | |
| 25 | 12 | 7.0 | 15.9 |
| 28 | 12 | 6.9 | 15.3 |
| 31 | 12 | 6.9 | 14.9 |
| Final pH of 2.65 | | | |
| 25 | 12 | 7.1 | 17.3 |
| 28 | 12 | 7.0 | 16.4 |
| 31 | 12 | 6.9 | 15.7 |

3.3. Effect of Temperature on the Structure of the DOPS/MO (2/8) Membrane in 50 mM NaCl. We examined the temperature-induced transitions of DOPS/MO (2/8) membranes in their suspension (5.5 mM lipid) at various final pH values from 2.50 to 2.75. The contour plot shows the SAXS patterns of DOPS/MO (2/8) membranes at pH 2.55 recorded during a temperature scan from 25 to 50 °C at a rate of 1 K/min (Figure 3a). At 25 °C, the SAXS peaks that have a spacing ratio of $\sqrt{2}:\sqrt{4}:\sqrt{6}$ were indexed as (110), (200), and (211) peaks of the Q_{II}^P phase (Figure 3b). At 32 °C, a new weak peak appeared around 0.170 nm^{-1} , and its intensity grew over time. At 50 °C, the peaks with a spacing ratio of $1:\sqrt{3}:2$ appeared, which corresponds to the H_{II} phase. Hence, the peak at 0.180 nm^{-1} was the (10) peak of the H_{II} phase. Thereby, this result indicates that a Q_{II}^P to H_{II} phase transition started to occur at 32 °C. At 50 °C, the peak intensity of the H_{II} phase became strong, but weak peaks due to the Q_{II}^P remained around 0.117 , 0.166 , and 0.203 nm^{-1} . At a final pH of 2.65, we obtained a similar result (Figure S1).

The lattice constant of the Q_{II}^P phase was almost constant at low temperatures, but above 29 °C, it decreased with temperature (Figure 3c). On the other hand, the lattice

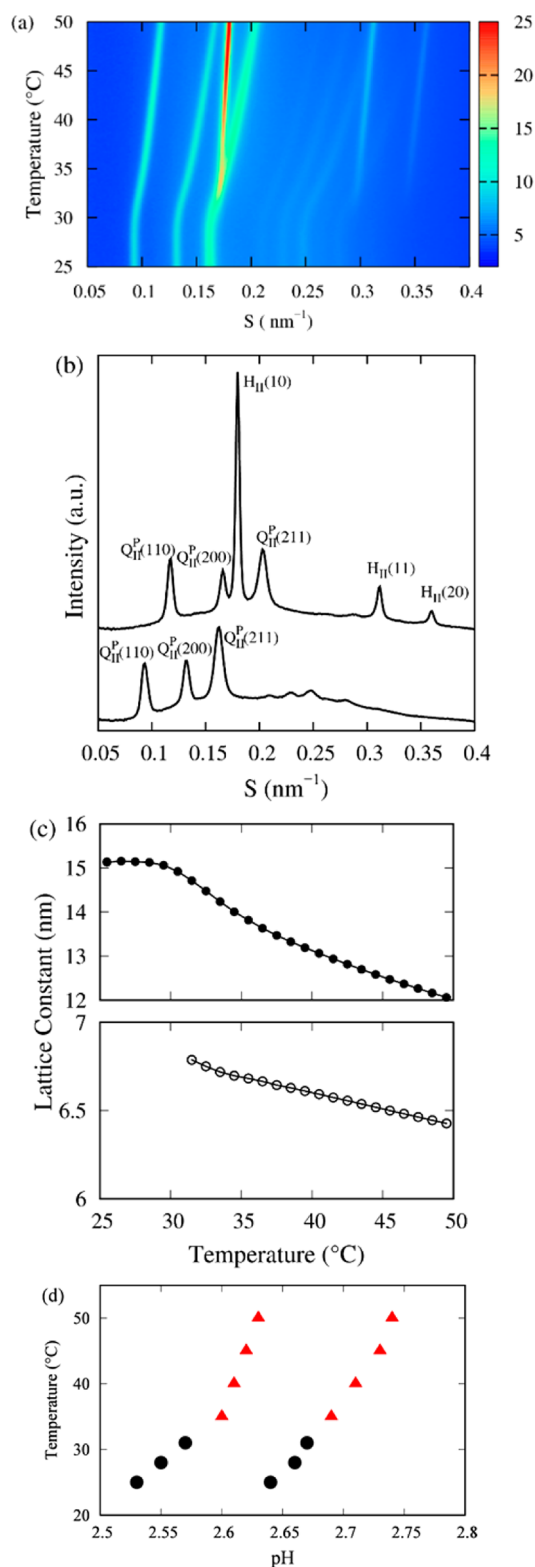


Figure 3. Changes in the structure and phase of DOPS/MO (2/8) membranes in 50 mM NaCl at low pH during a temperature scan from 25 to 50 °C at a rate of 1 °C/min. (a) SAXS contour plot of the temperature scan at a final pH of 2.55. (b) Averaged SAXS patterns of the data shown in panel a from 25.0 to 26.0 °C (bottom) and from 49.0 to 50.0 °C (top). (c) Temperature dependence of the lattice constants of the Q_{II}^P phase (top) and the H_{II} phase (bottom) at a final pH of 2.55. (d) Temperature–pH phase diagram: (circles) Q_{II}^P phase and (triangles) coexistence of the Q_{II}^P and H_{II} phases.

constant of the H_{II} phase decreased from 6.79 nm with an increase in temperature. This result agrees with the temperature dependence of the lattice constant of the H_{II} phase in other lipid membranes.^{51,52} On the basis of these SAXS experiments, we made the temperature–pH phase diagram (Figure 3d) after correction of the pH of the solution using data on the temperature dependence of the pH value (Figure S2). The Q_{II}^P to H_{II} phase transition occurred as the temperature increased, which agrees with the findings of other researchers.^{40,53}

3.4. Temperature Dependence of the Kinetics of the L_α to Q_{II}^P Phase Transition of the DOPS/MO (2/8) Membrane Induced by a Decrease in pH. Using the same method described in section 3.2, we examined the kinetics of the L_α to Q_{II}^P phase transition in a DOPS/MO (2/8) membrane when the pH was changed from neutral pH to a final pH of 2.65 at various temperatures. We already described the result at 25 °C (Figure 2c). The result of the same experiment at 31 °C (Figure 4a) shows that the peak of the H_{II}

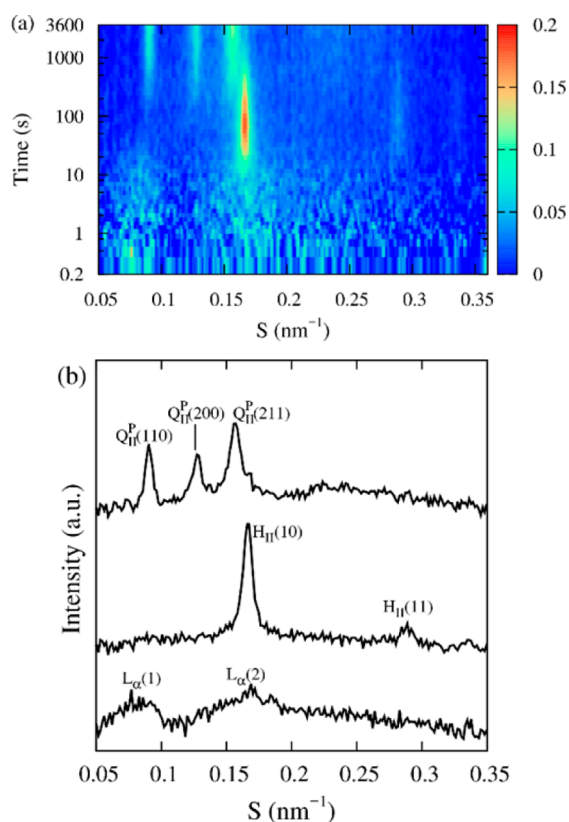


Figure 4. Changes in the structure and phase of DOPS/MO (2/8) membranes in 50 mM NaCl after the change in pH from pH 6.7 to a final pH of 2.65 at 31 °C. (a) SAXS contour plot of the time course. (b) Averaged SAXS patterns of the data shown in panel a from 0.2 to 9 s (bottom), from 50 to 89 s (middle), and from 2560 to 3629 s (top).

phase appeared earlier but the peaks of the Q_{II}^P phase appeared later compared with those at 25 °C (Figure 2c). At 31 °C (Figure 4a), the (10) peak of the H_{II} phase started to appear at ~ 10 s, but the (110) and (111) peaks of the Q_{II}^P phase started to appear at ~ 300 s. The lattice constant of the H_{II} phase decreased with temperature from 7.1 nm (at 25 °C) to 6.9 nm (31 °C) (Table 1).

We performed the same TR-SAXS experiments at a final pH of 2.55 at various temperatures and obtained similar results (see the quantitative analysis in the Discussion).

4. DISCUSSION

In this report, we found that an L_α to Q_{II}^P phase transition occurred in DOPS/MO (2/8) membranes in buffers containing 50 mM NaCl at and below the final pH of 2.75 when the pH of the MLV suspension decreased from neutral pH (Figure 1c). As we reported previously,^{22,43} in the same buffer containing 100 mM NaCl, a different phase transition, i.e., an L_α to Q_{II}^D phase transition, occurred in DOPS/MO (2/8) membranes. This difference can be explained as follows. The results of the salt concentration dependence of the membrane at pH 2.6 (Figure 1d) indicate that at <75 mM NaCl the Q_{II}^P phase is more stable than the Q_{II}^D phase. It is well-known that the level of EI in buffer increases with a decrease in salt concentration because the electric potential due to the membrane surface charges is screened by counterions and its degree of screening decreases with a decrease in salt concentration (i.e., the Debye length increases).³ Therefore, the result of Figure 1d indicates that the Q_{II}^P phase becomes more stable than the Q_{II}^D phase with an increase in the extent of EI. This is consistent with the general principle that as the EI due to surface charges increases the most stable phase of lipid membranes changes as follows: $Q_{II}^D \rightarrow Q_{II}^P \rightarrow L_\alpha$.^{11,12,18}

We also revealed the kinetic pathway of the L_α to Q_{II}^P phase transition in this membrane system induced by decreasing the pH to a low value. The first step is the rapid transition from the L_α phase to the H_{II} phase, and the second step is the slow transition from the H_{II} phase to the Q_{II}^P phase. To analyze the kinetics of this transition quantitatively, the NMF method^{49,50} was applied to obtain the time course of each phase.⁴³ The results of the analysis of the L_α to Q_{II}^P phase transition [final pH 2.55 at 25 °C (the result in Figure 2a)] are shown in Figure 5. Panels a–c of Figure 5 indicate three components in the data, i.e., the L_α , H_{II} , and Q_{II}^P phases, respectively. Panels d–f

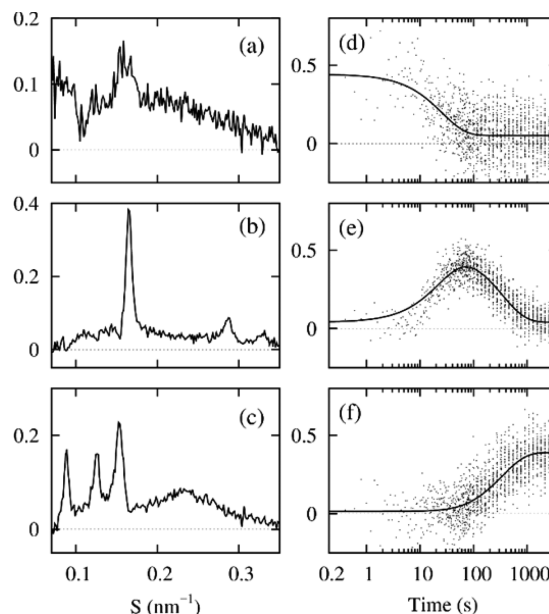


Figure 5. Results from the MALS calculations of the SAXS pattern of a DOPS/MO (2/8) membrane suspension in 50 mM NaCl from 0.2 to 3629 s after the change in pH from pH 6.7 to a final pH of 2.55 at 25 °C (Figure 2a). Restored SAXS profiles of matrix A corresponding to the L_α , H_{II} , and Q_{II}^P phases are shown in panels a–c, respectively. The time courses of the SAXS intensities of matrix B corresponding to the L_α , H_{II} , and Q_{II}^P phases are shown in panels d–f, respectively.

of Figure 5 show the changes in the SAXS intensities of each component, i.e., each phase, over time. There are two stages in the change. In the first step ($0 \leq t \leq 70$ s), the concentration of the L_α phase decreased, that of the H_{II} phases increased, and that of the Q_{II}^P phase remained almost zero, indicating that most of the membranes in the L_α phase converted to the H_{II} phase. In the second stage ($70 \text{ s} \leq t \leq 2000$ s), the concentration of the H_{II} phase decreased, that of the Q_{II}^P phase increased, and that of the L_α phase remained constant, indicating that the H_{II} phase converted to the Q_{II}^P phase. Therefore, we can reasonably consider the kinetic pathway of the transition as $L_\alpha \rightarrow H_{II} \rightarrow Q_{II}^P$. If we express that k_1 and k_2 are the rate constants of the L_α to H_{II} phase transition and of the H_{II} to Q_{II}^P phase transition, respectively, we can obtain the time courses of the concentration of each phase as follows according to our previous paper.⁴³

$$\begin{aligned} [L_\alpha] &= A_0 \exp(-k_1 t) + B_0 \\ [H_{II}] &= A_1 [\exp(-k_1 t) - \exp(-k_2 t)] + B_1 \\ [Q_{II}^P] &= A_2 [k_1 \exp(-k_2 t) - k_2 \exp(-k_1 t)] + B_2 \end{aligned} \quad (1)$$

The change in the SAXS intensities of the three phases over time (Figure 5d–f) was fit well by eq 1, providing a k_1 of 0.038 s^{-1} and a k_2 of 0.0029 s^{-1} . These results verify that the kinetic pathway of these phase transitions is $L_\alpha \rightarrow H_{II} \rightarrow Q_{II}^P$. Rate constant k_1 increased with a decrease in pH (Table 2), suggesting that the activation energy for the L_α to H_{II} phase transition decreases with a decrease in pH.

Table 2. pH Dependence of the Rate Constants

| temperature (°C) | pH 2.55 | pH 2.65 |
|--|-----------------------|---------------------|
| (a) k_1 (s^{-1}) (rate constants for the transition from the L_α phase to the H_{II} phase) | | |
| 25 | 0.038 ± 0.002 | 0.0134 ± 0.0008 |
| 28 | 0.058 ± 0.003 | 0.0285 ± 0.0015 |
| 31 | 0.068 ± 0.004 | 0.043 ± 0.002 |
| (b) k_2 (s^{-1}) (the rate constants of the transition from the H_{II} phase to the Q_{II}^P phase) | | |
| 25 | 0.0029 ± 0.0002 | 0.0030 ± 0.0002 |
| 28 | 0.0027 ± 0.0002 | 0.0032 ± 0.0002 |
| 31 | 0.00087 ± 0.00006 | 0.0016 ± 0.0001 |

Next we consider the temperature dependence of the rate constants of both steps. The k_1 values greatly increased with temperature for all pH values. Figure 6a shows the graphs of $\log_{10} k_1$ versus $1/T$ (where T is the absolute temperature) at various pH values. Because $k = A \exp(-E_a/RT)$, where E_a is the apparent activation energy that does not depend on temperature, R is the gas constant, and A is a constant called the pre-exponential factor, the value of E_a can be determined using the relation $-2.30R \times$ (slope of the curve of $\log_{10} k$ versus $1/T$). As temperature was increased from 25 to 31 °C, the pH of the suspension changed by <0.04 unit (Figure S3), and therefore, we approximated the constant pH from 25 to 31 °C. At all pH values, the data were well fit by a linear line, indicating that the apparent activation energy of the L_α to H_{II} phase transition, $E_a(L_\alpha \rightarrow H_{II})$, does not depend on temperature (i.e., is constant). Thereby, we were able to obtain the values of $E_a(L_\alpha \rightarrow H_{II})$ by the slope of the curves. The value of $E_a(L_\alpha \rightarrow H_{II})$ increased greatly with an increase in pH from 70 ± 20 kJ/mol at pH 2.55 to 150 ± 20 kJ/mol at pH 2.65 (Figure 6a, inset). The appearance of the intermediate H_{II} phase in the

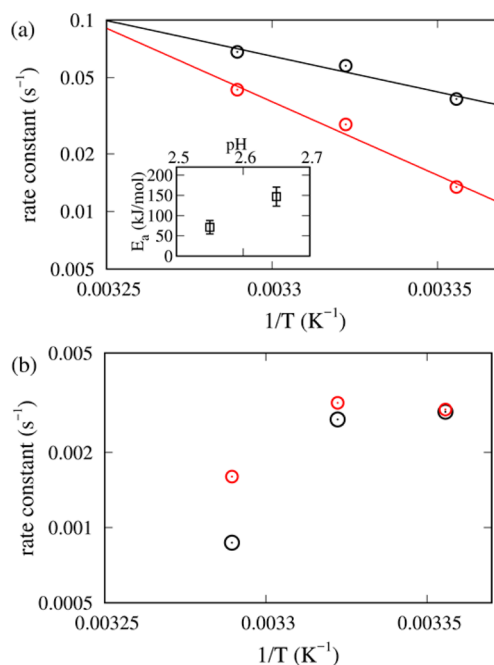


Figure 6. Temperature dependence of the rate constant. (a) $\log_{10} k_1$ vs $1/T$ at a final pH of 2.55 (black) and at pH 2.65 (red). The inset shows the pH dependence of apparent activation energy $E_a(L_\alpha \rightarrow H_{II})$. (b) $\log_{10} k_2$ vs $1/T$ at a final pH of 2.55 (black) and at pH 2.65 (red).

low-pH-induced L_α to Q_{II}^P phase transition can be explained by the activation energy of the direct transition from the L_α phase to the Q_{II}^P phase, $E_a(L_\alpha \rightarrow Q_{II}^P)$, being greater than that of the transition to the intermediate state, $E_a(L_\alpha \rightarrow H_{II})$. As shown in Table 2a, k_1 increased greatly with a decrease in pH at the same temperature, which can be explained by the decrease in $E_a(L_\alpha \rightarrow H_{II})$ with a decrease in pH (Figure 6a). Here we did not correct the pH (i.e., the pH in Figure 6 is the pH at 25 °C) but considered it as an experimental error in the values of E_a .

The result described above indicates that $E_a(L_\alpha \rightarrow H_{II})$ at pH 2.65 is 2-fold larger than that at pH 2.55. In the process of the L_α to H_{II} phase transition, at first neighboring bilayers in the L_α phase must contact each other at a local site because of their thermal fluctuation (see Figure S8a in the Supporting Information of ref 44), and then the apposed (cis) monolayers fuse to form stalk structures (or the trans monolayer contact) (Figure S8b in ref 44).^{54,55} We consider that the stalk structure involves the transition state, which determines $E_a(L_\alpha \rightarrow H_{II})$. The surface charge density of the DOPS/MO membrane increases with an increase in pH because the protonation of the carboxylic acid of DOPS becomes smaller at higher pH values. Therefore, we can reasonably consider that the level of EI inside the membrane in the stalk structure increases with an increase in pH, resulting in an increase in $E_a(L_\alpha \rightarrow H_{II})$.

We can compare the results of the phase transitions in 50 mM NaCl in this report with those of the phase transitions in 100 mM NaCl reported previously.⁴⁴ The $E_a(L_\alpha \rightarrow H_{II})$ value in 50 mM NaCl at pH 2.55 (i.e., 70 ± 20 kJ/mol) is almost the same as that in 100 mM NaCl (i.e., 60 ± 20 kJ/mol), but the $E_a(L_\alpha \rightarrow H_{II})$ value at pH 2.65 in 50 mM NaCl (i.e., 150 ± 20 kJ/mol) is slightly larger than that in 100 mM NaCl (i.e., 100 ± 50 kJ/mol) (Table 3). This comparison of $E_a(L_\alpha \rightarrow H_{II})$ can explain the results of k_1 ; k_1 (50 mM) ($=0.038 \text{ s}^{-1}$) was almost the same as k_1 (100 mM) ($=0.041 \text{ s}^{-1}$) at pH 2.55, and k_1 (50 mM) ($=0.013 \text{ s}^{-1}$) was slightly smaller than k_1 (100 mM)

Table 3. pH Dependence of the Apparent Activation Energy of the L_α to H_{II} Phase Transition, $E_a(L_\alpha \rightarrow H_{II})$

| | pH 2.55 | pH 2.65 | pH 2.75 |
|---------------------------|----------------|-----------------|-----------------|
| 50 mM NaCl | 70 ± 20 kJ/mol | 150 ± 20 kJ/mol | not determined |
| 100 mM NaCl ⁴⁴ | 60 ± 20 kJ/mol | 100 ± 40 kJ/mol | 160 ± 40 kJ/mol |

(=0.021 s⁻¹) at pH 2.65. Therefore, we can conclude that the EI effect due to the change in the NaCl concentration on $E_a(L_\alpha \rightarrow H_{II})$ is small, which is in contrast with the EI effect on the phase of the DOPS/MO membrane at equilibrium (Figure 1d). At present, we cannot explain this different effect reasonably.

In contrast, the value of k_2 of the second step of the phase transition decreased with temperature at pH 2.6 and 2.7 (Figure 6b and Table 2b). At both pH values, the k_2 values at 31 °C were much smaller than those at lower temperatures. For this reason, it may be considered the existence of a small amount of the H_{II} phase at equilibrium under the conditions that were used (i.e., coexistence of the Q_{II}^P and H_{II} phases). However, the data of the temperature scan (Figure 3a,c) indicate the absence of the H_{II} phase at 31 °C, and also the MALS data at 31 °C (Figure S2e) indicate that the SAXS intensity of the H_{II} phase decreased to the initial value at 3000 s. These results support the finding that the DOPS/MO (2/8) membranes at 31 °C are completely in the Q_{II}^P phase (no coexistence of the H_{II} phase). Therefore, the results of the decrease in k_2 values with temperature indicate that $E_a(H_{II} \rightarrow Q_{II}^P)$, which is defined by the slope of a tangent of the curve $\ln k_2$ versus $1/T$, is negative and its absolute value increased with temperature, although the number of data points is limited.

In our previous paper,⁴⁴ we have constructed a quantitative theory of the activation energy of phase transitions of lipid membranes, which was obtained by modification of the theory of Squires et al.,⁴⁵ including the effect of monolayer curvature. Using this new theory, we analyzed the experimental results of the L_α to Q_{II}^D phase transition in a DOPS/MO (2/8) membrane in 100 mM NaCl induced by a decrease in pH. The main point of this theory is that the free energy of the transition state, G^\ddagger , depends on temperature; in particular in our case, G^\ddagger increases greatly with temperature because G^\ddagger is involved in changes in monolayer curvature, and therefore, the (true) activation energy, $\Delta G^\ddagger (=G^\ddagger - G_A)$, where G_A is the free energy of initial phase A, of phase transitions of lipid membranes from phase A to phase B depends on temperature. According to the theory,⁴⁴ for the first step of the L_α to Q_{II}^P phase transition in a DOPS/MO (2/8) membrane (the L_α to H_{II} transition), if the mean curvature of the transition state, $H^\ddagger(L_\alpha \rightarrow H_{II})$, is constant (i.e., independent of temperature), $\Delta G^\ddagger(L_\alpha \rightarrow H_{II}) = bT + c$, where b and c are constants (i.e., eq 10 in ref 44 for $\beta = 0$). Because $k = A \exp[-\Delta G^\ddagger(T)/RT]$, the apparent activation energy of the first step, $E_a(L_\alpha \rightarrow H_{II})$, which was determined by experimental results shown in Figure 6a, is determined as follows

$$E_a(L_\alpha \rightarrow H_{II}) = -R \left[\frac{\partial \ln k}{\partial (1/T)} \right] = \Delta G^\ddagger - T \left(\frac{\partial \Delta G^\ddagger}{\partial T} \right) = c \quad (2)$$

Equation 2 indicates that $E_a(L_\alpha \rightarrow H_{II})$ does not depend on temperature, which agrees with the experimental results. On the other hand, according to the theory,⁴⁴ for the second step of

the L_α to Q_{II}^P phase transition in a DOPS/MO (2/8) membrane (the H_{II} to Q_{II}^P transition), $\Delta G^\ddagger(H_{II} \rightarrow Q_{II}^P) = a'T^2 + b'T + c'$, where a' , b' , and c' are constants (i.e., eq 14 in ref 44). Therefore, the apparent activation energy of the second step, $E_a(H_{II} \rightarrow Q_{II}^P)$, which was determined by experimental results shown in Figure 6b, is determined as follows

$$E_a(H_{II} \rightarrow Q_{II}^P) = -R \left[\frac{\partial \ln k}{\partial (1/T)} \right] = -a'T^2 + c' \quad (3)$$

where $a' = 2\kappa N_A N_{\text{coop}} A_n [(\alpha - \gamma)^2 - (\alpha - \beta)^2]$

where κ is the bending modulus of the monolayer, N_A is Avogadro's number, N_{coop} is the number of molecules in a cooperative unit,^{45,56} A_n is the cross-sectional area per molecule at the pivotal surface, and α , β , and γ are positive parameters representing the temperature dependence of the spontaneous curvature (H_0), the mean curvature of the H_{II} phase ($H_{H_{II}}$), and the transition state (H^\ddagger), respectively (i.e., $H_0 = -C_0 - \alpha T$, $H_{H_{II}} = -C_2 - \beta T$, and $H^\ddagger = -C_3 - \gamma T$, where C_0 , C_2 , and C_3 are positive constants). To agree with the experimental results [$E_a(H_{II} \rightarrow Q_{II}^P) < 0$], a' should be positive ($a' > 0$), and hence $(\alpha - \beta)^2 < (\alpha - \gamma)^2$. Generally, the absolute value of H_0 is larger than that of the mean curvature of the H_{II} phase and the transition state. Therefore, $|\alpha - \beta| < |\alpha - \gamma|$. This means that the difference between the temperature dependence of the curvature of the transition state and H_0 is greater than that between that of the curvature of the initial state (i.e., the H_{II} phase) and H_0 , indicating that G^\ddagger increases more than the free energy of the H_{II} phase, $G_{H_{II}}$, with an increase in temperature, and hence $\Delta G^\ddagger(H_{II} \rightarrow Q_{II}^P) (=G^\ddagger - G_{H_{II}})$ increases with temperature. In the temperature region that satisfies the relationship $a'T^2 > c'$, $E_a(H_{II} \rightarrow Q_{II}^P) < 0$. Under these conditions, $\Delta G^\ddagger(H_{II} \rightarrow Q_{II}^P)$ increases greatly with temperature, and as a result, the k_2 value decreases with an increase in temperature. Figure 6b indicates that $E_a(H_{II} \rightarrow Q_{II}^P) < 0$ and $|E_a(H_{II} \rightarrow Q_{II}^P)|$ increases with temperature, which agrees with the prediction of eq 3.

As we discussed in our previous paper, $\Delta G^\ddagger(L_\alpha \rightarrow H_{II})$ is proportional to N_{coop} (see eq 10 in ref 44). We have not yet succeeded in determining the value of N_{coop} in the process of the L_α to H_{II} transition, and thus, we represented the values of $E_a(L_\alpha \rightarrow H_{II})$ per mole. Therefore, the numerical values of $E_a(L_\alpha \rightarrow H_{II})$ in themselves are not important, but the comparison of them can be used.

The temperature range used for the determination of the apparent activation energy is very limited (i.e., from 25 to 31 °C), and therefore, the accuracy of their values is not so high [the significant figures of the apparent activation energy are only one or two; i.e., its relative error (fractional uncertainty) is 10–30% (Table 3)]. If we could increase the temperature range of the measurement and hence the number of data points, its significant figure would increase to two or three; i.e., its relative error is 1–5%. However, for the conclusion of this report, one or two significant figures is sufficient. The small temperature range of the measurement of the rate constant of the low-pH-induced phase transition is mainly due to the fact that the Q_{II} phase existed in a limited temperature range (from 25 to 32 °C) (Figure 3). We tried to measure the rate constant of phase transitions from 20 °C, but it turned out that the reproducibility of the rate constants was not good. This is likely due to hysteresis of the temperature change; in this

measurement, we prepared the samples at 25 °C and then decreased the temperature to 20 °C to measure phase transitions, but the involvement of the process in the decrease in temperature may induce the hysteresis probably due to its slow rate of transition.

When we started to investigate the low-pH-induced transitions between different Q_{II} phases and between the Q_{II} phase and other phases (the H_{II} and L_{α} phases) many years ago,¹¹ we did not consider any applications. At that time, we found that in oleic acid (OA)/MO (1/9) membranes as the pH decreased from a neutral value, a Q_{II}^P to Q_{II}^D phase transition occurred at pH 5.8 and then a Q_{II}^D to H_{II} phase transition occurred at pH 5.3.¹¹ After that, we found that in DOPS/MO (2/8) membranes as the pH decreased from a neutral value, an L_{α} to Q_{II}^D phase transition occurred at pH 2.9.²² This phase transition was reversible; i.e., as the pH increased from a low value, a Q_{II}^D to L_{α} phase transition occurred.²² We also found that DOPS/MO (2/8) large unilamellar vesicles (LUVs) were transformed into the Q_{II}^D phase as well as DOPS/MO (2/8) MLVs when the pH values of suspensions were decreased.²² Recently, several researchers found the applications of this principle of the low-pH-induced transitions between the Q_{II} and H_{II} phases,^{26,32} indicating that they are useful in targeted drug delivery and in cancer treatment. In this report, we found that in DOPS/MO (2/8) membranes low-pH-induced L_{α} to Q_{II} phase transitions occurred at various ion concentrations (Q_{II}^P phase at low ion concentrations and Q_{II}^D phase at higher ion concentrations). The pH values inducing these phase transitions were low (pH <3.0). Using these characteristics, we can apply these transitions to delivery of substances. We can prepare DOPS/MO (2/8) membrane LUVs or MLVs in the L_{α} phase containing chemical substances in their membrane hydrophobic core or bound to their membrane surface at neutral pH and deliver them to a specific place whose aqueous solution has a low pH. Then, the membranes can be transformed into bulk cubic phase membranes, which will float in an aqueous solution (due to their lower density) or be bound strongly to a surface of the specific place because the Q_{II}^D phase membranes are not soluble in water. Hence, they can provide these substances slowly in a specific place. For example, this pH-sensitive phase transition can be applied efficiently in a controlled release drug delivery system. DOPS/MO (2/8) membrane LUVs or MLVs containing drug molecules in their hydrophobic core or bound to their membrane interface at neutral pH can be transformed into the Q_{II}^D phase at gastric pH (1–3) after oral administration. This bulk cubic phase membrane has a density that is lower than that of gastric juice and can act as a buoyant dosage form or microballoon from which slow release of drug molecules can be achieved. This dosage form is useful in the treatment of *Helicobacter pylori* where prolonged local action is necessary in the gastroduodenal wall.⁵⁷ Generally, for drug delivery systems, nonbiological lipids have been used. However, DOPS, MO, and OA that were used in our studies are important biological lipids in mammals, including humans, that do not cause bodily harm. Before we started the investigation of the phase transitions of DOPS/MO membranes,²² we expected that a transition between the L_{α} and Q_{II} phases would occur around pH 4–5, but the results were different. We explained this reason by the change in pK values of DOPS in the membrane interface previously.²² If we could increase the pH values at which a low-pH-induced L_{α} to Q_{II} phase transition occurs, the range of its applications would be widened.

5. CONCLUSION

We found that an L_{α} to Q_{II}^P phase transition occurred in the DOPS/MO (2/8) membrane in buffers containing 50 mM NaCl at and below the final pH of 2.75 when the pH of the MLV suspension decreased. The kinetic pathway of this phase transition was revealed; the first step is the rapid transition from the L_{α} phase to the H_{II} phase, and the second step is the slow transition from the H_{II} phase to the Q_{II}^P phase. The rate constants of the first step increased with temperature. By analyzing this result, we obtained the values of its apparent activation energy, which did not change with temperature but increased with pH. This can be explained by an EI effect on the free energy of the transition state. In contrast, the rate constant of the second step decreased with temperature, indicating that the true activation energy increased with temperature. We analyzed these results using the theory of the activation energy of phase transitions of lipid membranes when the free energy of the transition state depends on temperature. The theory can reasonably explain these results qualitatively.

■ ASSOCIATED CONTENT

Supporting Information

The Supporting Information is available free of charge on the ACS Publications website at DOI: 10.1021/acs.langmuir.7b02512.

SAXS data of other conditions, MALS calculation of other conditions, and temperature dependence of the pH of membrane suspensions (PDF)

■ AUTHOR INFORMATION

Corresponding Author

*Nanomaterials Research Division, Research Institute of Electronics, Shizuoka University, 836 Oya, Suruga-ku, Shizuoka 422-8529, Japan. Telephone and fax: 81-54-238-4741. E-mail: yamazaki.masahito@shizuoka.ac.jp.

ORCID

Toshihiko Oka: 0000-0002-1676-9231

Masahito Yamazaki: 0000-0002-5959-9914

Present Address

[†]M.Z.I.: Department of Biotechnology and Genetic Engineering, Jahangirnagar University, Savar, Dhaka 1342, Bangladesh.

Notes

The authors declare no competing financial interest.

■ ACKNOWLEDGMENTS

This work was supported in part by a Grant-in-Aid for Scientific Research (B) (15H04361) from the Japan Society for the Promotion of Science (JSPS) to M.Y. Part of this research is based on a Cooperative Research Project of the Research Institute of Electronics, Shizuoka University. The synchrotron radiation experiments were performed using BL40B2 at SPring-8 with the approval of the Japan Synchrotron Radiation Research Institute (JASRI) (Proposals 2016A1192, 2016B1413, and 2017A1385) and BL-6A of the Photon Factory with the approval of the Photon Factory Advisory Committee (Proposal 2016G058). Preliminary SAXS experiments were performed at the Molecular Structure Analysis Section of Shizuoka University RIGST.

REFERENCES

- (1) McLaughlin, S.; Murray, D. Plasma membrane phosphoinositide organization by protein electrostatics. *Nature* **2005**, *438*, 605–612.
- (2) Zasloff, M. Antimicrobial peptides of multicellular organisms. *Nature* **2002**, *415*, 389–395.
- (3) Israelachvili, J. N. *Intermolecular and surface forces*, 2nd ed.; Academic Press: New York, 1992.
- (4) Tamba, Y.; Yamazaki, M. Magainin 2-induce pore formation in the lipid membranes depends of its concentration in the membrane interface. *J. Phys. Chem. B* **2009**, *113*, 4846–4852.
- (5) Karal, M. A. S.; Levadnyy, V.; Tsuboi, T.; Belaya, M.; Yamazaki, M. Electrostatic interaction effects on tension-induced pore formation in lipid membranes. *Phys. Rev. E* **2015**, *92*, 012708.
- (6) Seddon, J. M.; Templer, R. H. Polymorphism of lipid-water systems. In *Structure and dynamics of membranes*; Lipowsky, R., Sackmann, E., Eds.; Elsevier Science B.V.: Amsterdam, 1995; pp 97–160.
- (7) Luzzati, V. Biological significance of lipid polymorphism: the cubic phases. *Curr. Opin. Struct. Biol.* **1997**, *7*, 661–668.
- (8) Schwarz, U. S.; Gompper, G. Stability of inverse bicontinuous cubic phases in lipid-water mixtures. *Phys. Rev. Lett.* **2000**, *85*, 1472–1475.
- (9) Almsheerqi, Z. A.; Kohlwein, S. D.; Deng, Y. Cubic membranes: a legend beyond the Flatland of cell membrane organization. *J. Cell Biol.* **2006**, *173*, 839–844.
- (10) Oka, T. Transformation between inverse bicontinuous cubic phases of a lipid from diamond to primitive. *Langmuir* **2015**, *31*, 3180–3185.
- (11) Aota-Nakano, Y.; Li, S. J.; Yamazaki, M. Effects of electrostatic interaction on the phase stability and structures of cubic phases of monoolein/oleic acid mixture membranes. *Biochim. Biophys. Acta, Biomembr.* **1999**, *1461*, 96–102.
- (12) Li, S. J.; Yamashita, Y.; Yamazaki, M. Effect of Electrostatic Interactions on Phase Stability of Cubic Phases of Membranes of Monoolein/Dioleoylphosphatidic Acid Mixture. *Biophys. J.* **2001**, *81*, 983–993.
- (13) Barriga, H. M. G.; Tyler, A. I. I.; McCarthy, N. L. C.; Parsons, E. S.; Ces, O.; Law, R. V.; Seddon, J. M.; Brooks, N. J. Temperature and pressure tuneable swollen bicontinuous cubic phases approaching nature's length scales. *Soft Matter* **2015**, *11*, 600–607.
- (14) Tyler, A. I. I.; Barriga, H. M. G.; Parsons, E. S.; McCarthy, N. L. C.; Ces, O.; Law, R. V.; Seddon, J. M.; Brooks, N. J. Electrostatic swelling of bicontinuous cubic lipid phases. *Soft Matter* **2015**, *11*, 3279–3286.
- (15) Angelov, B.; Angelova, A.; Drechsler, M.; Garamus, V. M.; Mutafchieva, R.; Lesieur, S. Identification of large channels in cationic PEGylated cubosome nanoparticles by synchrotron radiation SAXS and Cryo-TEM imaging. *Soft Matter* **2015**, *11*, 3686–3692.
- (16) Cherezov, V.; Clogston, J.; Misquitta, Y.; Abdel-Gawad, W.; Caffrey, M. Membrane protein crystallization in meso: lipid type-tailoring of the cubic phase. *Biophys. J.* **2002**, *83*, 3393–3407.
- (17) Chupin, V.; Killian, J. A.; de Kruijff, B. Effect of phospholipids and a transmembrane peptides on the stability of the cubic phase of monoolein: implication for protein crystallization from a cubic phase. *Biophys. J.* **2003**, *84*, 2373–2381.
- (18) Masum, S. M.; Li, S. J.; Tamba, Y.; Yamashita, Y.; Tanaka, T.; Yamazaki, M. Effect of de novo designed peptides interacting with the lipid-membrane interface on the stability of the cubic phases of the monoolein membrane. *Langmuir* **2003**, *19*, 4745–4753.
- (19) Masum, S. M.; Li, S. J.; Awad, T. S.; Yamazaki, M. Effect of Positively Charged Short Peptides on Stability of Cubic Phases of Monoolein/Dioleoylphosphatidic Acid Mixtures. *Langmuir* **2005**, *21*, 5290–5297.
- (20) Awad, T. S.; Okamoto, Y.; Masum, S. M.; Yamazaki, M. Formation of cubic phases from large unilamellar vesicles of dioleoylphosphatidylglycerol/monoolein membranes induced by low concentrations of Ca²⁺. *Langmuir* **2005**, *21*, 11556–11561.
- (21) Yamazaki, M. Transformation between Liposomes and Cubic Phases of Biological Lipid Membranes Induced by Modulation of Electrostatic Interactions. *Adv. Planar Lipid Bilayers Liposomes* **2009**, *9*, 163–209.
- (22) Okamoto, Y.; Masum, S. M.; Miyazawa, H.; Yamazaki, M. Low pH-induced transformation of bilayer membrane into bicontinuous cubic phase in dioleoyl-phosphatidylserine/monoolein membranes. *Langmuir* **2008**, *24*, 3400–3406.
- (23) Pisani, M.; Fino, V.; Bruni, P.; Di Cola, E.; Francescangeli, O. Metal cation induced cubic phase in poly(ethylene glycol)-functionalized dioleoylphosphatidylethanolamine aqueous dispersions. *J. Phys. Chem. B* **2008**, *112*, 5276–5278.
- (24) Silva, J. P. N.; Oliveira, R.; Coutinho, P. J. G. Characterization of mixed DODAB/monoolein aggregates using Nile Red as a solvatochromic and anisotropy fluorescent probe. *J. Photochem. Photobiol., A* **2009**, *203*, 32–39.
- (25) Efrat, R.; Abramov, Z.; Aserin, A.; Garti, N. Nonionic-anionic mixed surfactants cubic mesophases. Part I: Structural chaotropic and kosmotropic effect. *J. Phys. Chem. B* **2010**, *114*, 10709–10716.
- (26) Negrini, R.; Mezzenga, R. pH-responsive lyotropic liquid crystals for controlled drug delivery. *Langmuir* **2011**, *27*, 5296–5303.
- (27) Muir, B. W.; Zhen, G.; Gunatillake, P.; Hartley, P. G. Salt induced lamellar to bicontinuous cubic phase transitions in cationic nanoparticles. *J. Phys. Chem. B* **2012**, *116*, 3551–3556.
- (28) Oliveira, I. M. S. C.; Silva, J. P. N.; Feitosa, E.; Marques, E. F.; Castanheira, E. M. S.; Real Oliveira, M. E. C. D. Aggregation behaviour of aqueous dioctadecyldimethylammonium bromide/monoolein mixtures: A multitechnique investigation on the influence of composition and temperature. *J. Colloid Interface Sci.* **2012**, *374*, 206–217.
- (29) Liu, Q.; Dong, Y.-D.; Hanley, T. L.; Boyd, B. J. Sensitivity of nanostructure in charged cubosomes to phase changes triggered by ionic species in solution. *Langmuir* **2013**, *29*, 14265–14273.
- (30) Hartnett, T. E.; Ladewig, K.; O'Connor, A. J.; Hartley, P. G.; McLean, K. M. Size and phase control of cubic lyotropic crystal nanoparticles. *J. Phys. Chem. B* **2014**, *118*, 7430–7439.
- (31) Liu, Q.; Wang, J.; Dong, Y.-D.; Boyd, B. J. Using a selective cadmium-binding peplipid to create responsive liquid crystalline nanomaterials. *J. Colloid Interface Sci.* **2015**, *449*, 122–129.
- (32) Negrini, R.; Fong, W.-K.; Boyd, B. J.; Mezzenga, R. pH-responsive lyotropic liquid crystals and their potential therapeutic role in cancer treatment. *Chem. Commun.* **2015**, *51*, 6671–6674.
- (33) Rodrigues, L.; Kyriakos, K.; Schneider, F.; Dietz, H.; Winter, G.; Papadakis, C. M.; Hubert, M. Characterization of lipid-based hexasomes as versatile vaccine carriers. *Mol. Pharmaceutics* **2016**, *13*, 3945–3954.
- (34) van't Hag, L.; Li, X.; Meikle, T. G.; Hoffmann, S. V.; Jones, N. C.; Pedersen, J. S.; Hawley, A. M.; Gras, S. L.; Conn, C. E.; Drummond, C. J. *Langmuir* **2016**, *32*, 6882–6894.
- (35) Squires, A. M.; Templer, R. H.; Seddon, J. M.; Woenckhaus, J.; Winter, R.; Finet, S.; Theyencheri, N. Kinetics and mechanism of the lamellar to gyroid inverse bicontinuous cubic phase transition. *Langmuir* **2002**, *18*, 7384–7392.
- (36) Cherezov, V.; Siegel, D. P.; Shaw, W.; Burgess, S. W.; Caffrey, M. The kinetics of non-lamellar phase formation in DOPE-Me: relevance to biomembrane fusion. *J. Membr. Biol.* **2003**, *195*, 165–182.
- (37) Kraineva, J.; Narayanan, R. A.; Kondrashkina, E.; Thiyagarajan, P.; Winter, R. Kinetics of lamellar-to-cubic and inter-cubic phase transitions of pure and cytochrome c containing monoolein dispersions monitored by time-resolved small-angle X-ray diffraction. *Langmuir* **2005**, *21*, 3559–3571.
- (38) Squires, A. M.; Templer, R. H.; Seddon, J. M.; Woenckhaus, J.; Winter, R.; Narayanan, T.; Finet, S. Kinetics and mechanism of interconversion of inverse bicontinuous cubic mesophase. *Phys. Rev. E* **2005**, *72*, 011502.
- (39) Conn, C. E.; Ces, O.; Mulet, X.; Finet, S.; Winter, R.; Seddon, J. M.; Templer, R. H. Dynamics of structural transformations between lamellar and inverse bicontinuous cubic lyotropic phases. *Phys. Rev. Lett.* **2006**, *96*, 108102.
- (40) Mulet, X.; Gong, X.; Waddington, L. J.; Drummond, C. J. Observing self-assembled lipid nanoparticles building order and

complexity through low-energy transformation processes. *ACS Nano* **2009**, *3*, 2789–2797.

(41) Angelova, A.; Angelov, B.; Garamus, V. M.; Couvreur, P.; Lesieur, S. Small-angle X-ray scattering investigations of biomolecular confinement, loading, and release from liquid-crystalline nanochannel assemblies. *J. Phys. Chem. Lett.* **2012**, *3*, 445–457.

(42) Alam, M. M.; Oka, T.; Ohta, N.; Yamazaki, M. Kinetics of Low pH-Induced Lamellar to Bicontinuous Cubic Phase Transition in Dioleoylphosphatidylserine/Monoolein. *J. Chem. Phys.* **2011**, *134*, 145102.

(43) Oka, T.; Tsuboi, T.; Saiki, T.; Takahashi, T.; Alam, J. M.; Yamazaki, M. Initial step of pH-jump-induced lamellar to bicontinuous cubic phase transition in dioleoylphosphatidylserine/monoolein. *Langmuir* **2014**, *30*, 8131–8140.

(44) Oka, T.; Saiki, T.; Alam, J. M.; Yamazaki, M. Activation energy of low-pH-induced lamellar to bicontinuous cubic phase transition in dioleoylphosphatidylserine/monoolein. *Langmuir* **2016**, *32*, 1327–1337.

(45) Squires, A. M.; Conn, C. E.; Seddon, J. M.; Templer, R. H. Quantitative model for the kinetics of lyotropic phase transitions involving changes in monolayer curvature. *Soft Matter* **2009**, *5*, 4773–4779.

(46) Marsh, D. Intrinsic curvature in normal and inverted lipid structures and in membranes. *Biophys. J.* **1996**, *70*, 2248–2255.

(47) Kinoshita, K.; Li, S. J.; Yamazaki, M. The mechanism of the stabilization of the hexagonal II (H_{II}) phase in phosphatidylethanolamine membranes in the presence of low concentrations of dimethyl sulfoxide. *Eur. Biophys. J.* **2001**, *30*, 207–220.

(48) Bartlett, G. R. Phosphorous assay in column chromatography. *J. Biol. Chem.* **1959**, *234*, 466–468.

(49) Paatero, P.; Tapper, U. Positive matrix factorization: A non-negative factor model with optimal utilization of error estimates of data values. *Environmetrics* **1994**, *5*, 111–126.

(50) Wang, J.-H.; Hopke, P. K.; Hancewicz, T. M.; Zhang, S. L. Application of modified alternating least squares regression to spectroscopic image analysis. *Anal. Chim. Acta* **2003**, *476*, 93–109.

(51) Koynova, R.; Caffrey, M. Phase and phase-transitions of the hydrated phosphatidylethanolamines. *Chem. Phys. Lipids* **1994**, *69*, 1–34.

(52) Qiu, H.; Caffrey, M. The phase diagram of the monoolein/water system: metastability and equilibrium aspects. *Biomaterials* **2000**, *21*, 223–234.

(53) Shyamsunder, E.; Gruner, S. M.; Tate, M. W.; Turner, D. C.; So, P. T. C.; Tilcock, C. P. S. Observation of inverted cubic phases in hydrated dioleoylphosphatidylethanolamine membranes. *Biochemistry* **1988**, *27*, 2332–2336.

(54) Siegel, D. P.; Epand, R. M. The mechanism of lamellar-to-inverted hexagonal phase transitions in phosphatidylethanolamine: implications for membrane fusion mechanisms. *Biophys. J.* **1997**, *73*, 3089–3111.

(55) Siegel, D. P. The modified stalk mechanism of lamellar/inverted phase transitions and its implications for membrane fusion. *Biophys. J.* **1999**, *76*, 291–313.

(56) Schöppe, A.; Hinz, H. – J.; Gerdes, R.; Redlich, H.; Rapp, G. Activation energies and kinetics of glycolipid phase transitions. *Chem. Phys. Lipids* **1999**, *103*, 95–115.

(57) Bardonnnet, P. L.; Faivre, V.; Pugh, W. J.; Piffaretti, J. C.; Falson, F. Gatroretentive dosage forms: Overview and special case of *Helicobacter pylori*. *J. Controlled Release* **2006**, *111*, 1–18.